ACSNANO

www.acsnano.org

ARTICLE

Correlating Interlayer Spacing and Separation Capability of Graphene Oxide Membranes in Organic Solvents

Sunxiang Zheng, Qingsong Tu, Monong Wang, Jeffrey J. Urban, and Baoxia Mi*

Cite This: *ACS Nano* 2020, 14, 6013–6023

Read Online

ACCESS | Metrics & More | Article Recommendations | Supporting Information

ABSTRACT: **Membranes synthesized by stacking two-dimensional graphene oxide (GO) hold great promise for applications in organic solvent nanofiltration. However, the performance of a layer-stacked GO membrane in organic solvent nanofiltration can be significantly affected by its swelling and interlayer spacing, which have not been systematically characterized. In this study, the interlayer spacing of the layer-stacked GO membrane in different organic solvents was experimentally characterized by liquid-phase ellipsometry. To understand the swelling mechanism, the solubility parameters of GO were experimentally determined and used to mathematically predict the Hansen solubility distance between GO and solvents, which is found to be a good predictor for GO swelling and interlayer spacing. Solvents with a small solubility distance (e.g., dimethylformamide, *N*-methyl-2-pyrrolidone) tend to cause significant GO swelling, resulting in an interlayer spacing of up to 2.7 nm. Solvents with a solubility distance larger than 9.5 (e.g., ethanol, acetone, hexane, and toluene) only cause minor swelling and are thus able to maintain an interlayer spacing of around 1 nm. Correspondingly, GO membranes in solvents with a large solubility distance exhibit good separation performance, for example, rejection of more than 90% of the small organic dye molecules (e.g., rhodamine B and methylene blue) in ethanol and acetone. Additionally, solvents with a large solubility distance result in a high slip velocity in GO channels and thus high solvent flux through the GO membrane. In summary, the GO membrane performs better in solvents that are unlike GO, i.e., solvents with large solubility distance.**

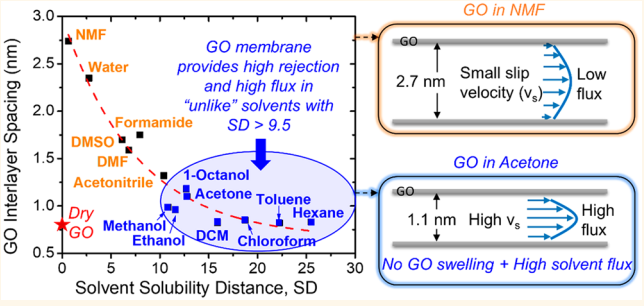

KEYWORDS: *graphene oxide, membrane, interlayer spacing, swelling, solubility distance, organic solvent nanofiltration*

The layer-stacked two-dimensional (2D) graphene oxide (GO) thin film has been intensively studied as a selective transport barrier in many important applications including gas separation,[1,2] water purification,[3,4] supercapacitors,[5] and batteries.[6] The surface of GO consisting of continuous hexagonal carbon lattice is considered impermeable to even the smallest molecules such as H_2 and H_2O,[7] while the nanosized channels formed naturally by self-stacking between two adjacent GO layers provide pathways for selective mass transport.[8] Since GO has excellent chemical stability in organic solvents, it has great potential to make selective membranes for separation in organic solvents such as acetone, dimethylformamide (DMF), and hexane that are frequently used in the petrochemical, food processing, and pharmaceutical industries.[9] Similar to its role in aqueous phase separation, the interlayer spacing, defined as the center-to-center distance between two adjacent carbon lattices, is essential for the targeted performance of the layer-stacked GO membrane in organic solvents.[10,11] However, most studies on the interlayer spacing of GO membranes and the mechanism of mass transport through a GO membrane are limited to the gaseous and aqueous phase separation, whereas there is no similar research on GO membranes in organic solvents.

Although the interlayer spacing of GO in liquid solvents can be measured using X-ray diffraction (XRD), this technique is usually not compatible with the presence of bulk liquid, often requiring sophisticated sample preparation. In addition to direct measurement of interlayer spacing, indirect characterization has also been attempted by measuring the change in the

Received: February 22, 2020
Accepted: May 7, 2020
Published: May 7, 2020

https://dx.doi.org/10.1021/acsnano.0c01550
ACS Nano 2020, 14, 6013–6023

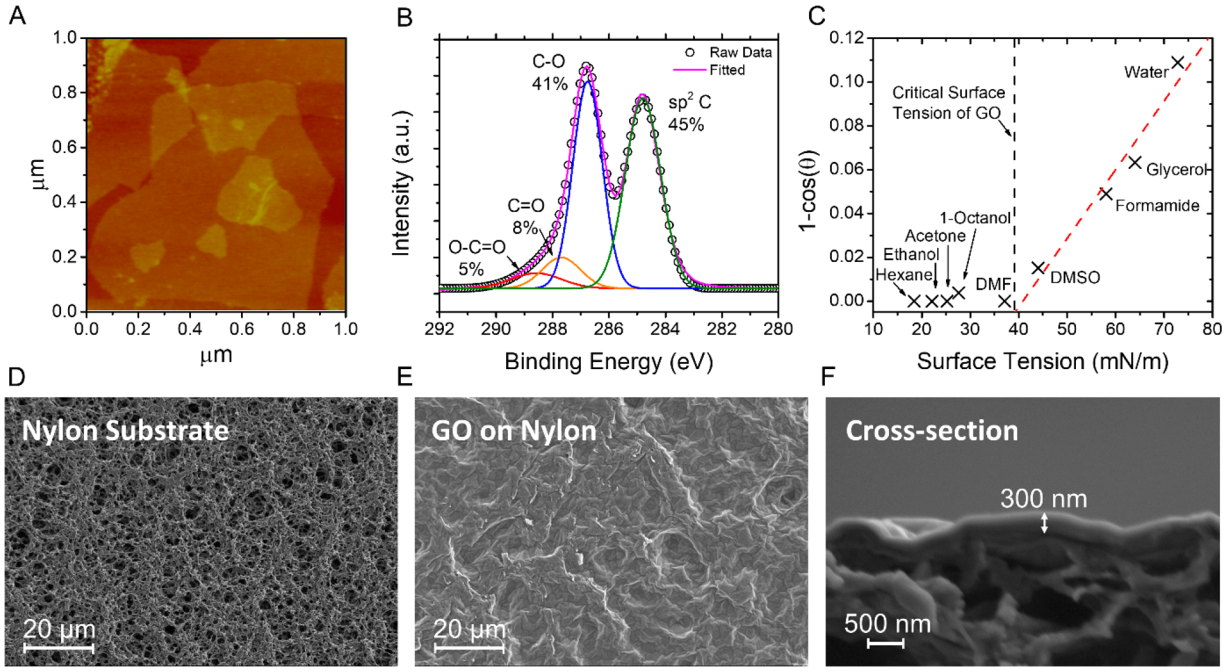

Figure 1. Physicochemical properties of GO nanosheets and the layer-stacked GO membrane. AFM image of the as-synthesized GO nanosheets (A). XPS characterization of the as-synthesized GO nanosheets confirming the abundance of oxygenated functional groups (B). Zisman plot to extrapolate the critical surface tension of GO (DMSO denotes for dimethyl sulfoxide) (C). SEM images of the top surface of the bare Nylon substrate (D), the top surface of the GO membrane (E), and the cross section of the GO membrane (F).

total thickness of the GO film soaked in bulk liquid, under the assumption that the isotropic increase of interlayer spacing in the thickness direction is proportional to the total thickness change. For example, the swelling of the GO membrane in aqueous solutions can be quantified with this approach using a pressurized contact thickness gauge[12] or, more accurately, liquid-phase ellipsometry.[13] This approach can be adapted to measure GO swelling in organic solvents, which would offer key knowledge to the understanding of transport mechanisms and the prediction of membrane separation performance. However, no systematic effort has been reported to the best of our knowledge.

The interlayer spacing of the GO film under dry conditions was reported to be around 0.7 nm,[7,14] which, if remaining unchanged during operation, would be ideal to filter out molecules that present the most challenges in the organic solvent separation processes (200 to 1000 Da).[15] However, once soaked in liquid, a GO film could potentially swell due to the interaction with solvent molecules,[16] compromising its rejection performance. For example, a GO membrane can swell severely during aqueous phase separation due to the high affinity between water molecules and the polar functional groups on the GO surface,[17] in terms of the strong short-range hydration force and long-range electrostatic repulsion force between two adjacent GO layers.[18−20] As a result, the interlayer spacing of a non-cross-linked GO membrane could increase to up to 6−7 nm in pure water and around 2 nm in salt water,[13] resulting in deteriorated selectivity.[21] However, the behavior and the underlying mechanism of GO swelling in aqueous solutions may not be the same as that in organic solvents. This is because the electrostatic interaction between GO layers weakens dramatically and becomes almost negligible in many organic solvents, and hence the swelling of layer-stacked GO membranes is much less pronounced, especially in nonpolar organic solvents such as hexane and toluene due to their low affinity to the GO surface.[22] Therefore, it is anticipated that GO membranes likely exhibit a very different swelling behavior and separation performance in different organic solvents, and research is warranted to fundamentally understand and theoretically quantify the interlayer spacing of the GO membrane in organic solvents.

In addition, the transport of organic solvents in a confined 2D GO nanochannel may exhibit distinct properties, which cannot be observed in the bulk.[23−25] For example, water molecules can form a high-density (~1.3 g/cm^3), well-aligned water network in a 2D GO nanochannel, as theoretically predicted and experimentally detected in our previous study.[13] Such an ordered water structure induced by van der Waals interactions between the graphitic regions of GO and water molecules potentially promotes fast water transport through the GO membrane.[26] Similarly, a recent theoretical study also predicts an enhanced transport of organic solvents in the 2D GO nanochannel due to the fast slippage of solvent molecules on the graphene surface.[27] Therefore, the interactions between solvent molecules and the GO surface can affect the slip velocity and thus the permeability of the solvent through the GO membranes. Such effects need to be well understood and quantified in order to systematically optimize the layer-stacked GO membrane for the best separation performance in organic solvents.

To help fill the above knowledge gaps, this study characterized the interlayer spacing of the layer-stacked GO membrane in organic solvents by using a liquid-phase ellipsometer and described the GO membrane swelling behavior by using the regular solution theory based on the solubility of GO in organic solvents. The performance of the GO membrane in organic solvents was tested in a pressurized nanofiltration membrane system. Molecular dynamics (MD) simulations were carried out to fundamentally understand the solvent transport mechanism in the 2D GO nanochannel.

https://dx.doi.org/10.1021/acsnano.0c01550
ACS Nano 2020, 14, 6013−6023

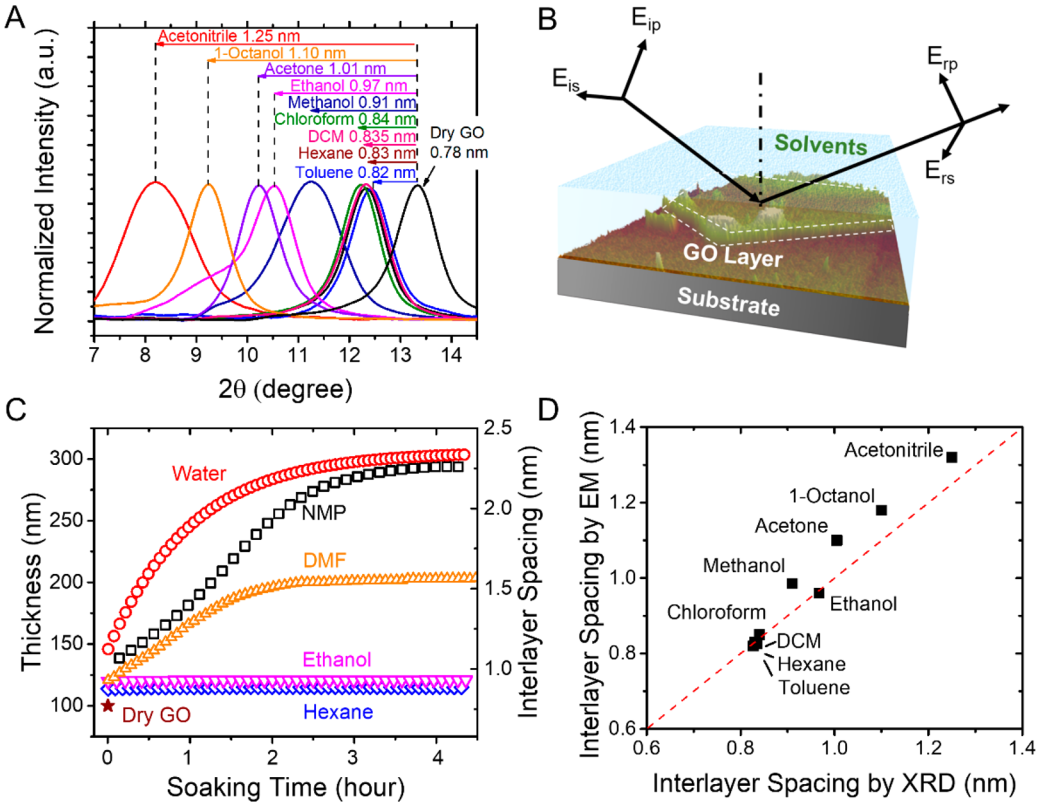

Figure 2. Characterization of the interlayer spacing of GO membranes in organic solvents. The XRD measurements of interlayer spacing of GO membranes after being soaked in various solvents (A). Schematic illustration of the liquid-phase ellipsometry as an alternative method to characterize the interlayer spacing of GO membranes being soaked in solvents. The optical measurement approach is based on the polarization from incident light E_{is} and E_{ip} to reflected light E_{rs} and E_{rp} (B). Characterization of the swelling kinetics of GO in selected solvents by the liquid-phase ellipsometer (C). The comparison of interlayer spacing obtained from the ellipsometer (EM) and XRD in selected organic solvents (D). The red dashed line is a visual guidance to demonstrate identical interlayer spacing obtained from EM and XRD. DCM, NMP, and DMF stand for dichloromethane, *N*-methyl-2-pyrrolidone, and dimethylformamide, respectively.

RESULTS AND DISCUSSION

Physiochemical Properties of GO Membranes. The GO nanosheets used to prepare GO membranes were synthesized using the modified Hummers' method.[3] The lateral size of the synthesized GO nanosheets was around 800 nm, measured using dynamic light scattering (Figure S1). Some small GO nanosheets with a lateral size down to 100 nm were also observed in AFM images (Figure 1A). The depth profile of the AFM images of the GO nanosheets shows that the GO nanosheets were mostly monolayers with a thickness around 1 nm. The degree of GO oxidation greatly affects the surface properties (e.g., wettability and surface charge) and potentially the interlayer spacing of GO in organic solvents. Therefore, the GO oxidation was characterized by XPS spectroscopy. As shown in Figure S2, the GO nanosheets were highly oxidized after chemical oxidation and ultrasonic exfoliation, exhibiting an O/C ratio of around 0.4. Figure 1B shows that around 45% of the carbon atoms on GO remained unoxidized, and the other 55% of the carbon atoms were associated with oxygenated functional groups such as hydroxyl, epoxide, and carboxylic groups. The presence of ionizable oxygenated functional groups on GO nanosheets makes GO negatively charged in aqueous solutions with pH greater than 4 (Figure S3). The negative charge is known to play a very important role in increasing membrane hydrophilicity and selectivity due to electrostatic effects in the aqueous environment.[28]

However, the surface charge of GO in organic solvents is very different from that in water. The dissociation of oxygenated functional groups in organic solvents is greatly suppressed due to relatively poor proton transfer capability.[29] For example, it has been reported that the pK_a of carboxylic groups, which serve as the main source of negative charges on GO, increases drastically in organic solvents.[30] Such a pK_a shift is linearly proportional to the inverse of the dielectric constant of the organic solvent according to the Born theory of ionic solvation.[31] The dielectric constant of most organic solvents is lower than that of water. Therefore, GO in these organic solvents tends to exhibit neutral or weak negative charges. As confirmed by the charge measurements in Figure S4A, the zeta potential of GO in organic solvents with a small dielectric constant (e.g., DMF, ethanol, and hexane) is in the range of −20 mV to 0 mV, much weaker than its zeta potential of −40 mV in water. However, in solvents with a higher dielectric constant (e.g., formamide, NMF) the zeta potential of GO (ranging between −21 mV and −25 mV) is still surprisingly weaker than in water. In order to explain why, we measured the conductivity of the organic solvents. As shown in Figure S4B, the conductivities of NMF and formamide are 296 μS cm^{-1} and 254 μS·cm^{-1}, respectively, much higher than other solvents (typically ranging between 0 and 4 μS·cm^{-1}). The high conductivity is likely caused by ionic impurities as both NMF and formamide are known to contain trace amounts of hydrolysis products.[32] The ionic impurities could screen the

https://dx.doi.org/10.1021/acsnano.0c01550
ACS Nano 2020, 14, 6013−6023

surface charge of GO due to the ionic strength effect, thus resulting in an unexpectedly weak zeta potential in NMF and formamide.

In addition to the surface charge, the wettability of GO membranes in organic solvents is also important for determining the membrane performance such as solvent permeability.[33] Typically, solvents would experience an increase in transport resistance at the liquid−solid interface of hardly wettable membranes.[34] As shown in Figure S5, the wettability of GO can be characterized by using a tensiometer to measure the contact angle of solvents on the smooth surface of a GO membrane deposited on a glass substrate. The equilibrium contact angles of nonpolar solvents (e.g., hexane) and some polar solvents (e.g., ethanol and acetone) are almost zero, and the contact angle of water is the largest (28°). Figure 1C shows the Zisman plot of a typical GO membrane surface, from which the critical surface tension of wetting on the GO surface is calculated to be 39 mN/m. In other words, solvents that have a surface tension lower than 39 mN/m (e.g., DMF, 1-octanol, ethanol, acetone, hexane) are expected to completely wet the membrane surface with negligible interfacial transport resistance. Thus, the observed good wettability indicates the potential of the membrane to achieve a high solvent flux.

Prior to layer-stacking GO nanosheets to make the membrane, the GO suspension was sonicated and centrifuged to ensure a uniform dispersion of GO monolayer nanosheets. The GO nanosheets were then deposited on a Nylon membrane support by vacuum filtration to form a layer-stacked GO membrane. As shown in Figure 1D, the bare Nylon substrate had interconnected pores with diameters of around 0.2 μm, which is considered incapable of rejecting small organic molecules. After the GO deposition, a continuous, smooth film was formed with a thickness of around 300 nm (Figure 1E,F), completely blocking the large pores in Nylon. As a result, the separation capability of the membrane would be governed by the structure and properties of the layer-stacked GO film.

Characterization of Interlayer Spacing by XRD and Liquid-Phase Ellipsometry. The interlayer spacing of layer-stacked GO in the dry condition can be conveniently characterized by XRD.[16,35] Nonoxidized graphite has an interlayer spacing of 0.34 nm,[36] which is almost equal to the van der Waals thickness of a single layer of carbon atoms.[37] Due to the presence of oxygenated functional groups protruding from the carbon lattice, the interlayer spacing of GO increases to 0.78 nm. The interlayer spacing of GO after being immersed in organic solvents may expand due to the intrusion of solvent molecules into the channels between GO nanosheets, resulting in the swelling of the GO membrane at the macroscopic scale. In this study, the swelling of the GO membrane after being soaked in organic solvents for 24 h to equilibrate was characterized by XRD. Figure 2A shows the shift of the XRD peak from an interlayer spacing of 0.78 nm in the initial dry state to 0.82−1.2 nm in selected organic solvents. Note that it becomes extremely challenging to obtain repeatable XRD data when the GO swelling goes beyond a certain threshold (~1.3 nm). The results agree well with previously reported values.[38] It was found that the GO membrane did not swell much in nonpolar solvents (e.g., hexane and toluene) but did swell dramatically in polar solvents (e.g., acetonitrile).

Large interlayer spacing, which is caused by the significant swelling of GO in solvents and beyond the measurement range of XRD, can be measured by liquid-phase ellipsometry. As another advantage, ellipsometry can measure the interlayer spacing of a sample while it is immersed in solvents, whereas XRD requires that the sample be taken out of the solvent prior to measurement. To carry out the swelling measurement using ellipsometry, a 100 nm-thick GO membrane was deposited on a substrate by a transplanting method described in our previous study (Figure 2B).[39] The GO-coated substrate was then mounted in a customized cell with a side window. E_{ip} and E_{is} shine on the GO membrane and polarize into E_{rp} and E_{rs} while being reflected to a detector. The thickness of the GO membrane in solvents can be monitored *in situ* and calculated using the Cauchy equation, as described in the SI and Figure S6. Then, the average interlayer spacing of GO in solvents ($d_{solvents\text{-}GO}$) is calculated as

$$d_{solvents\text{-}GO} = d_{Dry\text{-}GO} \times \frac{\tau_{solvents\text{-}GO}}{\tau_{Dry\text{-}GO}} \quad (1)$$

where $\tau_{solvents\text{-}GO}$ and $\tau_{Dry\text{-}GO}$ are the total thickness of the GO membrane in solvents and in the dry state, respectively.

As shown in Figure 2C, the GO membrane did not swell at all after being soaked in ethanol and hexane for at least 4 h. However, the thickness of GO increased dramatically within the first 2 h of soaking in water, NMP, and DMF, indicating fast swelling due to the adsorption of solvents into the GO layers. The swelling stopped or became much slower after 4 h. To examine the accuracy of ellipsometry measurements, we compared the interlayer spacing measured by ellipsometry to that by XRD. As shown in Figure 2D, the interlayer spacing obtained by ellipsometry is up to 10% larger than that obtained by XRD, and the difference is more apparent when the GO membrane swells. This is most likely because ellipsometry measures the average interlayer spacing of GO over large regions while XRD only measures the interlayer spacing of GO in well aligned regions.

Understanding the Interlayer Spacing of GO in Organic Solvents. The quantitative prediction of membrane swelling in organic solvents is challenging.[40,41] It has been demonstrated that GO swelling in aqueous solutions can be well modeled by the Derjaguin−Landau−Verwey−Overbeek (DLVO) theory.[13] The interlayer spacing of the GO layers in aqueous solutions is determined by the thickness of the electrical double layer, which is defined as the following Debye length λ_D:

$$\lambda_D = \sqrt{\frac{\varepsilon_s \varepsilon_0 kT}{2N_A e^2 I}} \quad (2)$$

where ε_s is the dielectric constant of solution, ε_0 the vacuum permittivity, k the Boltzmann constant, T the absolute temperature; N_A the Avogadro number; e the electron charge, and I the ionic strength of the bulk solution. Using this model, the dielectric constant of the solution correlates well with the swelling degree of the laminar structure.[42,43] However, such a linear correlation may not be true in the case of organic solvents, for which it has been reported that swelling is either not observed when the dielectric constant is below a threshold or reaches a plateau when the dielectric constant exceeds a certain value.[44,45] The plot of the measured interlayer spacing of GO in organic solvents vs the dielectric constant of solvents in Figure S7 shows a relatively poor correlation between the

https://dx.doi.org/10.1021/acsnano.0c01550
ACS Nano 2020, 14, 6013−6023

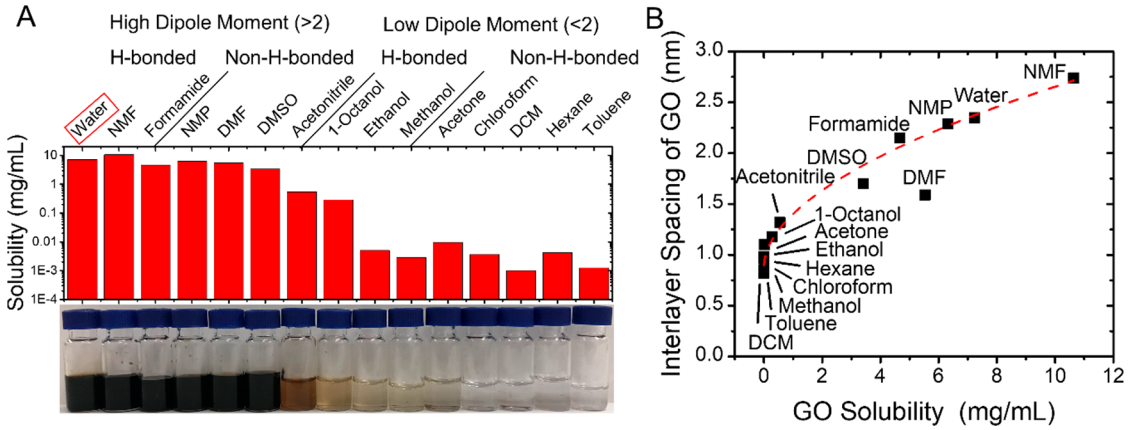

Figure 3. Experimentally measured solubility of GO in selected solvents (A) and its strong correlation with the interlayer spacing of GO obtained from ellipsometry measurements (B).

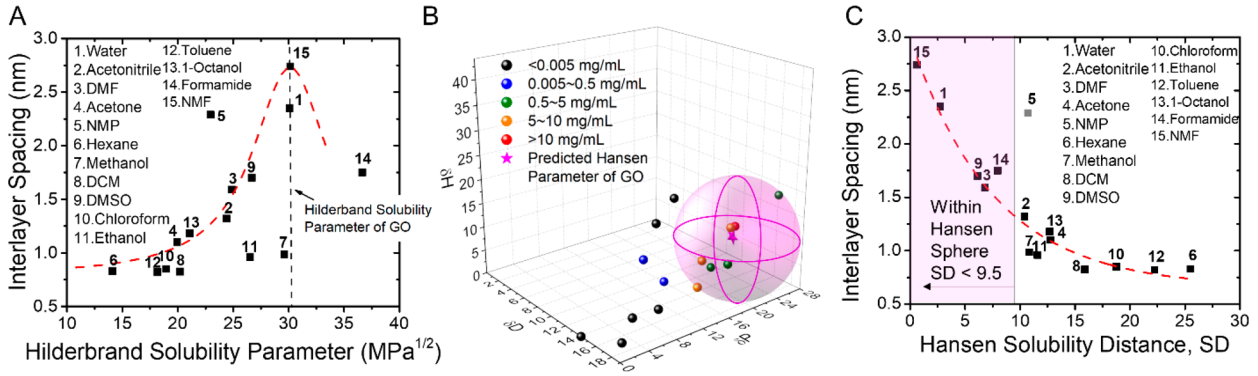

Figure 4. Prediction of the swelling/interlayer spacing of GO based on solubility parameters. Correlation between the interlayer spacing of GO and the Hildebrand solubility parameter (A). Illustration of the Hansen space based on the Hansen solubility parameters of solvents and the predicted values of GO (B). Hansen sphere is represented by the pink sphere with a center at GO (pink star) and a radius of 9.5. The solvents with Hansen solubility distance (SD) < 9.5 are located within the Hansen sphere, and the solvents with SD > 9.5 are located outside of the Hansen sphere. Correlation between the interlayer spacing of GO in different solvents and their Hansen solubility distance, SD (C).

two. Therefore, the DLVO model is not applicable in the case of organic solvents due to the change in the electrical double layer,[46,47] calling for an alternative model to fully explain/predict GO swelling in organic solvents.

The age-old saying of "like dissolve like" indicates that GO swelling is likely to be strongly affected by its solubility in organic solvents. The solubility parameters and dipole moments of selected solvents are summarized in Table S1. We experimentally measured the solubility of GO in these solvents. As shown in Figure 3A, GO dissolved much better in polar solvents (e.g., DMF, NMP) than in nonpolar ones (e.g., hexane, toluene). Polar solvents such as DMSO, DMF, and NMP, which have a high dipole moment, i.e., strong dipole−dipole intermolecular interactions, result in high GO solubility, indicating that dipole−dipole interactions are a governing factor in determining GO solubility. In addition, the formation of the hydrogen bond (H-bond) also contributes to the GO solubility in solvents. For instance, polar protic solvents (e.g., water and formamide) can form a strong H-bond with oxygenated functional groups on GO, resulting in high GO solubility, while polar aprotic solvents (e.g., DMSO, DMF, NMP, and acetonitrile) can only be the acceptor of protons, thus having a weaker capability of forming the H-bond and dissolving GO. In nonpolar solvents, GO barely dissolves because neither H-bond nor dipole−dipole interactions are present. The low solubility of GO in nonpolar solvents also reveals that the nonpolar interactions are not capable of dissolving GO.

The measured solubility of GO in each of the 15 different solvents is plotted against the interlayer spacing of GO in the corresponding solvent in Figure 3B, which shows a strong correlation between the two. Solvents that can keep a large quantity of GO nanosheets suspended result in a large interlayer spacing in the GO membrane, suggesting that the interlayer spacing of the GO membrane may be estimated based on the regular solution theory. Under some assumptions, this theory has proved highly capable of predicting the swelling of polymers in organic solvents.[48−50] It has also been used to predict the swelling of layered montmorillonite,[51] hinting its feasibility in describing the swelling of the layer-stacked 2D nanomaterial.

To develop a universal model to predict the swelling of GO in different solvents, first we need to determine the solubility parameters of GO. Based on the traditional dissolution theory developed by Hildebrand,[52] the molar energy change ΔE of mixing two components with a negligible total volume change can be calculated as

$$\Delta E = V_m \alpha_1 \alpha_2 (\delta_1 - \delta_2)^2 \quad (3)$$

where α_1 and α_2 are the volume fractions of the two components and δ_1 and δ_2 the Hildebrand solubility

https://dx.doi.org/10.1021/acsnano.0c01550
ACS Nano 2020, 14, 6013−6023

parameters of the two components. The Hildebrand solubility parameter δ is defined as

$$\delta = \left(\frac{\Delta_g U}{V_m}\right)^{1/2} \quad (4)$$

where $\Delta_g U$ is the energy required to vaporize one mole of the pure component and V_m is the molar volume.

It is challenging to obtain the Hildebrand solubility parameter of GO because, unlike pure solvents, GO has no quantifiable vapor pressure as needed to determine $\Delta_g U$ in eq 4. Therefore, we developed an alternative approach to estimate the solubility parameter of GO in this study. As suggested by eq 3, the maximum solubility can be obtained when GO has a similar solubility parameter to that of the solvent. This is because as the Hildebrand solubility parameters of the two components are close to each other (i.e., $\delta_1 - \delta_2$ approaches zero), ΔE is minimized, and the mixing of the two components results in the highest solubility. Figure 3B demonstrates that GO has the highest solubility in *N*-methylformamide (NMF) among the 15 representative solvents, suggesting that the Hildebrand solubility parameter of GO is close to that of NMF, which is around 30 $MPa^{1/2}$.

However, the Hildebrand solubility parameter of GO alone is not a good predictor for GO swelling. As observed in Figure 4A, there is an overall variation trend for most solvents (identified by the red dashed line) except a few outliers. In general, the interlayer spacing of GO in NMF was the largest (~2.7 nm) and decreased considerably when the Hildebrand solubility parameter deviated from 30 $MPa^{1/2}$. The least swelling occurred in hexane and toluene, which have Hildebrand solubility parameters below 20 $MPa^{1/2}$, deviating the most from 30 $MPa^{1/2}$. However, in ethanol and DMSO, which have similar Hildebrand solubility parameters (26.5 and 26.7 $MPa^{1/2}$) to that of GO (30 $MPa^{1/2}$), very different swelling behavior was observed, i.e., the interlayer spacings of GO in ethanol and DMSO were 0.96 and 1.7 nm, respectively. This is most likely because multiple intermolecular interactions coexist, so use of the single Hildebrand solubility parameter cannot completely explain the swelling of GO.

To account for the different intermolecular interactions that contribute to the overall solubility and swelling of GO, the Hildebrand solubility parameter can be further split into three Hansen solubility parameters, i.e., the dispersion cohesive parameter δ_D, the polar cohesive parameter δ_P, and the H-bond parameter δ_H, as expressed in following equation.

$$\delta^2 = \delta_D{}^2 + \delta_P{}^2 + \delta_H{}^2 \quad (5)$$

where each Hansen solubility parameter δ_i of GO can be estimated by using the solubility-weighted average as given in eq 6.

$$\delta_{i,GO} = \frac{\sum S_{solvent}\delta_{i,solvent}}{\sum S_{solvent}} \quad (6)$$

where $S_{solvent}$ is the experimentally tested solubility of GO in a given solvent and $\delta_{i,solvent}$ is a Hansen solubility parameter for each solvent and available in the literature.

Using eq 6, the Hansen solubility parameters of GO, $\delta_{D,GO}$, $\delta_{P,GO}$, and $\delta_{H,GO}$, are calculated to be 17.5 $MPa^{1/2}$, 19.1 $MPa^{1/2}$, and 15.4 $MPa^{1/2}$, respectively, which are generally consistent with those reported by Konios et al.,[53] except that our δ_P value is higher by 10 $MPa^{1/2}$, a discrepancy that might be a result of the different oxidation degrees of GO used in different studies. Figure 4B illustrates the Hansen space spanned by the dimensions of δ_D, δ_P, and δ_H. The Hansen solubility parameters of GO determine the center (star symbol in Figure 4B) of a sphere, which is the so-called Hansen solubility sphere (pink sphere in Figure 4B). If a solvent is located within the sphere, it is a good solvent for dissolving GO (solubility > 0.5 mg/mL) and outside a poor solvent (solubility < 0.5 mg/mL). For visual convenience, the 3D Hansen space can also be translated into a two-dimensional plot (Figure S8), where we find the polar−polar interactions (high dipole and hydrogen bond) contribute the most to the solubility of GO, implying the importance of oxygenated functional groups to the solubility and swelling of GO in organic solvents.

To quantitatively use the Hansen solubility sphere, we define a Hansen solubility distance (SD) as the distance between the two points given by the solvent coordinates ($\delta_{D,solvent}$, $\delta_{P,solvent}$, $\delta_{H,solvent}$) and the GO coordinates ($\delta_{D,GO}$, $\delta_{P,GO}$, $\delta_{H,GO}$), respectively, as below

$$SD^2 = 4(\delta_{D,GO} - \delta_{D,solvent})^2 + (\delta_{P,GO} - \delta_{P,solvent})^2 + (\delta_{H,GO} - \delta_{H,solvent})^2 \quad (7)$$

The radius of the Hansen sphere is estimated to be ~9.5, indicating that a solvent that has an SD < 9.5, i.e., within a distance of 9.5 units from the point of GO in the Hansen space, could be considered a good solvent for GO.

The Hansen solubility distance SD is plotted against the GO interlayer spacing in Figure 4C, which clearly shows that the interlayer spacing of GO decreases exponentially with the increase of SD; i.e., GO swells less as the solubility distance increases. However, NMP (point 5) appeared to cause more dramatic swelling than predicted, possibly due to some other interactions beyond the ones described by Hansen solubility parameters. Indeed, NMP contains a lactam structure that is reported to have $\pi-\pi$ interactions with the aromatic rings on GO.[54] Nevertheless, we find that the Hansen solubility distance SD is the best predictor for the swelling and interlayer spacing of GO. The SD approach could be universally applied to the understanding of the solubility and swelling of other emerging 2D nanomaterials (e.g., MoS_2, boron nitride, and titanium carbide) in organic solvents.

Mechanisms of Solvent Flux and Mass Transport in GO Membranes. The separation performances (i.e., solvent flux and solute rejection) of the layer-stacked GO membrane in organic solvents were tested in a pressurized nanofiltration system. Before each test, the GO membrane was soaked in a solvent for at least 6 h to reach an equilibrium interlayer spacing. Despite drastic GO swelling in some solvents, no delamination of GO was observed during the soaking or testing (Figure S9). For a pressure-driven flow, the solvent transport through two parallel GO nanosheets can be described by the Hagen−Poiseuille equation for viscous flow assuming a no-slip boundary condition:

$$J = \frac{d^4 \Delta P}{12\eta W^2 L} \quad (8)$$

where the solvent flux J is a function of the distance d between two nanosheets (i.e., the interlayer spacing of GO), the nanosheet width W (i.e., lateral size of GO, ~800 nm), the total thickness of the GO membrane L (~300 nm), the applied pressure ΔP, and the solvent viscosity η.

https://dx.doi.org/10.1021/acsnano.0c01550
ACS Nano 2020, 14, 6013−6023

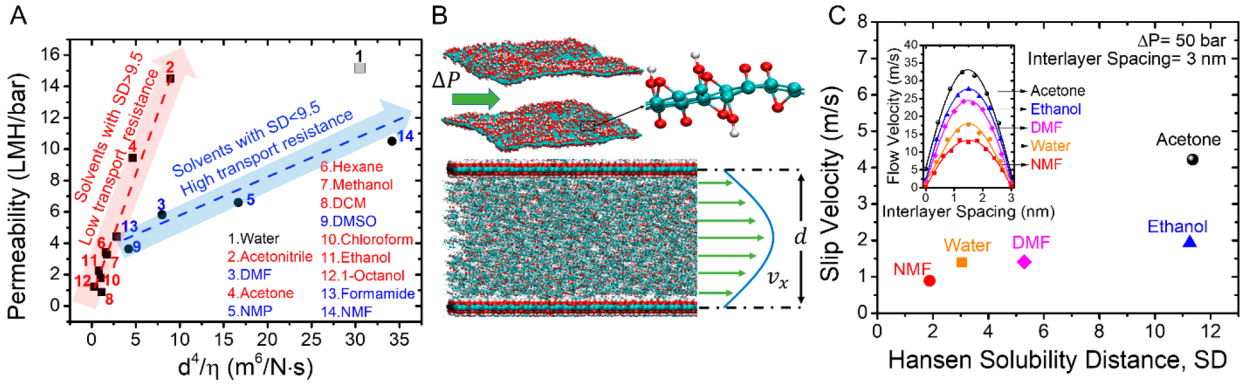

Figure 5. Mechanisms of solvent transport in the GO membrane. The effect of solvent properties (d^4/η) and Hansen solubility distance (SD) on the permeability of solvents through the GO membrane (A). Schematic illustration of molecular dynamics modeling of solvent transport between two parallel GO nanosheets under a transmembrane pressure of ΔP (B). The interlayer spacing of the modeled GO nanosheets is fixed at 3 nm. Effect of the Hansen solubility distance (SD) on the slip velocity of the selected solvents (C). The inset illustrates the representative flow velocity profiles of different solvents in the GO channel.

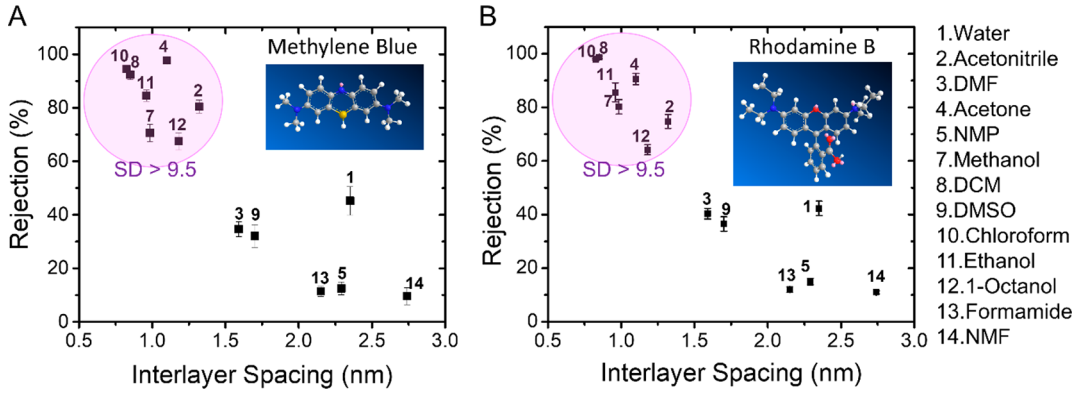

Figure 6. Rejection of methylene blue (A) and rhodamine B (B) by the GO membrane in different organic solvents. The feed solution contains 100 ppm methylene blue or rhodamine B. Insets are the chemical structures of methylene blue and rhodamine B.

Equation 8 describes a linear correlation between solvent permeability ($J/\Delta P$) and an integrated parameter (d^4/η) determined by the interlayer spacing of GO and solvent viscosity. Therefore, the plot of permeability vs d^4/η in Figure 5A is expected to give a constant slope ($1/W^2L$, because the lateral size of GO (W) and membrane thickness (L) are fixed parameters. However, Figure 5A shows that the data points form two groups that exhibit drastically different slopes, that is, a relatively steep slope for solvents with a large Hansen solubility distance (SD > 9.5) indicating low transport resistance and a relatively gentle slope for solvents with a small Hansen solubility distance (SD < 9.5) indicating high transport resistance. We hypothesize that this is because the difference in the boundary slip velocities of solvents is not accounted for in eq 8, but instead, a slip velocity of zero is assumed for all solvents. Large slip velocity has been reported for water transport in graphene channels, but the slip velocity and hence water flux decreases significantly after the graphene is decorated with oxygenated functional groups that induce strong interactions with water.[55] Similarly, the strong interactions between GO and solvents with small Hansen solubility distance results in high friction and hence a decrease in the slip velocity.

To verify our hypothesis, we conducted molecular dynamics simulation of the solvent transport in confined GO nanochannels, as described in detail in the SI. Figure 5B shows the construction of two GO nanosheets in parallel with an interlayer spacing of 3 nm. The GO nanosheets are decorated with oxygenated functional groups, including 20% of hydroxyl and 33% of epoxy as characterized by XPS (Figures 1B and S10). The introduction of solvents into the system allows the interlayer spacing of GO nanosheets to be adjusted so as to achieve a minimum system energy. A pressure gradient of 50 bar is applied along the GO nanochannel to drive the solvent transport. The velocity profile in Figure 5C exhibits a characteristic parabolic velocity distribution, with the slip velocity at the boundary being greater than zero. The simulation results in Figure 5C demonstrate that solvents with higher solubility distance SD, such as acetone and ethanol, have higher slip velocity and thus lower transport resistance and higher permeability than solvents with lower SD. In other words, if a solvent "dislikes" the GO nanosheets (i.e., one with a large SD), it permeates fast in GO.

To understand the separation capability of the GO membrane in different organic solvents, we tested the rejection of two types of dyes, i.e., rhodamine B (RB, MW 479 g/mol) and methylene blue (MB, MW 320 g/mol). As shown in Figure 6A,B, the rejection of dyes dissolved in chloroform and DCM, which do not cause membrane swelling, can reach over 90%. The rejection decreases as the interlayer spacing increases, indicating a strong correlation between the size of the GO nanochannel and the membrane separation capability. In addition to the size effect, the solute separation by the GO membrane can also be affected by partition-diffusion effects,

https://dx.doi.org/10.1021/acsnano.0c01550
ACS Nano 2020, 14, 6013−6023

i.e., solute partitioning into the GO channel followed by hindered diffusion through the channel. We evaluated the partitioning of RB into GO membranes from a few selected solvents (Figure S11) and found poor correlations with the rejection of RB. Therefore, the separation mechanisms in GO membranes are likely dominated by size exclusion and hindered diffusion.

In rejection induced by hindered diffusion, the relative affinity of dye molecules toward GO and solvents plays an important role. For example, the rejection of RB and MB in acetone is consistently higher than that in ethanol, although the GO membrane has a slightly larger interlayer spacing in acetone (~1.1 nm) than that in ethanol (~0.96 nm). To understand the affinity, we measured the solubilities of RB and MB in different organic solvents (Figure S12). If the affinity between the dye molecules and the membrane is greater than the affinity between the dye molecules and the solvents, the dye molecules tend to stay with the membrane rather than with the solvent and diffuse at a much slower rate than in the solvent, resulting in higher rejection. For example, the solubility of MB in ethanol was measured to be 102 mg/mL (Figure S12), which is 1000 times that in acetone, revealing a dramatically higher affinity between MB and ethanol. As a result, MB is much easier to be carried by ethanol than by acetone through the GO membrane to the permeate side.

As the interlayer spacing of GO increased to over 2 nm, we observed less than 10% rejection of the dye in organic solvents since the size of the dye molecules is estimated to be around 1 nm. Interestingly, we found that the rejection of RB and MB in water was much higher (~40%) than in organic solvents. A plausible reason is that electrostatic interaction is more pronounced in water as opposed to that in the organic solvents. Both RB and MB are positively charged in water at neutral pH and hence can be electrostatically attracted to the negatively charged GO nanosheets. Such electrostatic attraction could potentially enhance the membrane selectivity by imposing additional diffusion hindrance through the 2D GO channels.

Implication for GO Membrane Design and Application. The result of this study has significant implications for the GO membrane synthesis and applications in organic phase separation such as the emerging organic solvent nanofiltration. We have demonstrated that the GO membrane can have very different swelling behaviors in a variety of organic solvents and that the equilibrium interlayer spacing can be predicted by the Hansen solubility distance. The interlayer spacing of GO significantly affects the selectivity of GO membranes. Therefore, for applications in solvents that cause significant GO swelling, stabilizing methods such as cross-linking need to be used in GO membrane synthesis, at the cost of compromised permeability and a relatively complex process. In addition, compared to some state-of-the-art organic solvent nanofiltration membranes in the literature (Table S2), the layer-stacked GO membrane in this study has comparable separation capability in acetone and exhibits 10-times higher permeability, suggesting a great potential of GO membranes in personal care products and pharmaceutical applications for which acetone is an important solvent. Moreover, this study has revealed that the oxidation degree of GO affects its solubility parameter and accordingly the swelling of GO in organic solvents. Therefore, the performance of the GO membrane can be potentially improved by finely tuning the degree of GO oxidation during synthesis or by partial reduction.

CONCLUSIONS

The Hansen solubility distance between GO and solvents is found to be a good predictor for GO swelling, interlayer spacing, and separation performance. In general, the GO membrane performs better in solvents that are unlike GO, i.e., solvents with a large solubility distance. Solvents with a small solubility distance tend to cause significant GO swelling, resulting in large interlayer spacing, low rejection of organic dyes, and low solvent flux. In unlike solvents with a solubility distance larger than 9.5 (e.g., ethanol, acetone, hexane, and toluene), GO membranes are able to maintain a small interlayer spacing, high rejection of small organic dyes, and high solvent flux.

METHODS

Chemicals. All chemicals were used as received from Sigma-Aldrich (St. Louis, MO) unless noted otherwise. The chemicals used in the present study included H_2O_2, H_2SO_4, $NaNO_3$, Na_2SO_4, graphite, acetone, acetonitrile, ethanol, methanol, 1-ocatanol, hexane, toluene, chloroform, dichloromethane (DCM), *N*-methyl-2-pyrrolidone (NMP), dimethylformamide (DMF), dimethyl sulfoxide (DMSO), *N*-methylformamide (NMF), formamide, methylene blue, and rhodamine B. GO was prepared from graphite flakes using the modified Hummers method with a procedure detailed in our earlier work.[3]

Characterization of the GO Membrane. X-ray photoelectron spectroscopy (XPS, PHI 5400, PerkinElmer, Eden Prairie, MN) was used to characterize the elemental composition of GO. Atomic force microscope (AFM, Dimension Icon, Bruker, Santa Barbara, CA) images were taken to characterize the thickness and lateral dimension of GO monolayers deposited on a silicon wafer. The contact angles of solvents on the GO membrane surface were measured using an optical tensiometer (Theta Lite, Biolin Scientific, Sweden). Scanning electron microscopy (SEM, Ultra-55 FESEM, ZEISS) images were taken for the surface of the Nylon substrate before and after GO coating. Cross-sectional images were obtained to evaluate the thickness of the GO coating. The zeta potential of the GO nanosheets in aqueous solutions was measured using a Zetasizer Nano-ZSP analyzer (Malvern, Westborough, MA). The interlayer spacings of GO in the dry state and in solvents were characterized by X-ray diffraction (XRD, Bruker D8 Discover GADDS) with a graphite-monochromated Co Kα radiation (λ = 0.179 nm).

Interlayer Spacing Measurement via Liquid-Phase Ellipsometry. A multiwavelength ellipsometer (FS-1Multi-wavelength, Film Sense, Lincoln, NE) was equipped with a cross-flow chamber (Biolin, Sweden) to allow the optical measurement through the window on each side of the chamber while maintainng a steady cross-flow through the chamber driven by a peristaltic pump. A gold-coated quartz disc (Biolin, Sweden) was used as the substrate for the GO layers. The optical properties of the gold substrate in the dry state and in the solvents were first measured in the chamber as a baseline. Cross flow of the solvents was kept at 1 mL/min to mimic the fluid condition in a real filtration system. The GO aqueous suspension was diluted and filtrated through a poly(ether sulfone) (PES, Sterlitech, Kent, WA) membrane to form a 100 nm-thick GO film. To coat the GO, the gold substrate was placed upside down on the GO-coated PES membrane, with its top surface contacting the GO film. The GO film was then transplanted onto the gold disc after peeling the disc off the membrane surface. The optical properties of the GO-coated substrate in the dry state and in the solvents were characterized using the ellipsometer. The ellipsometry data were analyzed with an established optical model. In general, data collected for the GO-coated substrate were fitted using Cauchy's equation to determine the thickness of the GO film in the dry state and in the solvents using the optical constants (i.e., refractive index and extinction index) of the solvent as the ambient parameters. More information about data analysis is provided in the SI.

https://dx.doi.org/10.1021/acsnano.0c01550
ACS Nano 2020, 14, 6013−6023

GO Solubility in Solvents. Dry GO powder was first acquired by drying the GO aqueous suspension in a freeze-dryer (FreeZone, Labconco). Then the GO powder was collected and redissolved into various solvents to measure solubility. To maximize GO dissolution in each solvent, GO powder was overdosed in the solvent and sonicated in a bath sonicator. The GO suspension in each solvent was subsequently centrifuged twice to remove undissolved GO solids. The GO solubility is thus obtained by measuring the concentration of the supernatant using a UV−vis spectrophotometer (Genesys 10S UV−vis, Thermo fisher) and a standard curve. The standard curve was established by first dissolving 1 mg of GO powder in 1 mL of selected solvent, then performing a serial dilution to obtain standard GO solutions with known concentrations, followed by measuring the UV absorption of the standard GO solutions at a characteristic peak of 350 nm, and finally generating the curve by plotting adsorption against the concentration of GO.

GO Membrane Preparation and Separation Performance Tests in Organic Solvents. Layer-stacked GO membranes were prepared by filtrating the GO aqueous suspension through a Nylon membrane substrate (Whatman, 0.2 μm pore size). The GO membranes were dried thoroughly in a vacuum oven at 60 °C for 24 h. To completely wet the GO membranes and achieve an equilibrium swelling, the GO membranes were soaked in the testing solvents for 12 h prior to the testing. Solvent flux and rejection performance of the GO membranes were evaluated in a pressurized stainless-steel stir cell. To achieve a steady permeation and rejection ratio, the GO membrane was first compressed under a high pressure of 70 psi (483 kPa) for stabilization. Data were then collected under 50 psi (345 kPa). The concentrations of organic dye in feed, permeate, and retentate solutions were measured by a UV−vis spectrophotometer. To make sure that the rejection performance is not due to adsorption, filtration tests were performed for at least 2 h to reach a steady state. The steady state was achieved by taking permeate samples at a certain time interval until the concentration difference between two samples was within 1%. The rejection R of markers is calculated using $R = \left(1 - \frac{C_P}{C_R}\right) \times 100\%$, where C_P and C_R are the concentrations of markers in the permeate and retentate solutions, respectively.

ASSOCIATED CONTENT

Supporting Information

The Supporting Information is available free of charge at https://pubs.acs.org/doi/10.1021/acsnano.0c01550.

> Characterization of the sizes, oxidation degrees, and charge properties of GO in aqueous solutions and organic solvents; wettability of the GO membrane surface by organic solvents; details on the ellipsometry measurement and data analysis; solubility parameters and dipole moments of selected solvents; correlation of the interlayer spacing of GO with the dielectric constant and solubility parameter; integrity of GO membranes in selected solvents; details on molecular dynamic simulation; and comparison of membrane performance for organic solvent nanofiltration (PDF)

AUTHOR INFORMATION

Corresponding Author

Baoxia Mi − *Department of Civil and Environmental Engineering, University of California, Berkeley, California 94720, United States;* orcid.org/0000-0003-3185-1820; Email: mib@berkeley.edu

Authors

Sunxiang Zheng − *Department of Civil and Environmental Engineering, University of California, Berkeley, California 94720, United States*

Qingsong Tu − *Department of Civil and Environmental Engineering, University of California, Berkeley, California 94720, United States;* orcid.org/0000-0002-2345-799X

Monong Wang − *Department of Civil and Environmental Engineering, University of California, Berkeley, California 94720, United States*

Jeffrey J. Urban − *The Molecular Foundry, Lawrence Berkeley National Laboratory, Berkeley, California 94720, United States;* orcid.org/0000-0002-6520-830X

Complete contact information is available at: https://pubs.acs.org/10.1021/acsnano.0c01550

Notes

The authors declare no competing financial interest.

ACKNOWLEDGMENTS

The material is based upon work supported by U.S. National Science Foundation (NSF) under Award Nos. CBET-1565452 and CBET-1706059 and the U.S. Department of Energy under Award No. DE-IA0000018. Work at the Molecular Foundry was supported by the Office of Science, Office of Basic Energy Sciences, of the U.S. Department of Energy under Contract No. DE-AC02-05CH11231. The opinions expressed herein, however, are those of the authors and do not necessarily reflect those of the sponsors.

REFERENCES

(1) Li, H.; Song, Z.; Zhang, X.; Huang, Y.; Li, S.; Mao, Y.; Ploehn, H. J.; Bao, Y.; Yu, M. Ultrathin, Molecular-Sieving Graphene Oxide Membranes for Selective Hydrogen Separation. *Science* **2013**, *342*, 95−98.

(2) Kim, H. W.; Yoon, H. W.; Yoon, S.-M.; Yoo, B. M.; Ahn, B. K.; Cho, Y. H.; Shin, H. J.; Yang, H.; Paik, U.; Kwon, S.; Choi, J.-Y.; Park, H. B. Selective Gas Transport Through Few-Layered Graphene and Graphene Oxide Membranes. *Science* **2013**, *342*, 91−95.

(3) Hu, M.; Mi, B. Enabling Graphene Oxide Nanosheets as Water Separation Membranes. *Environ. Sci. Technol.* **2013**, *47*, 3715−3723.

(4) Huang, K.; Liu, G. P.; Lou, Y. Y.; Dong, Z. Y.; Shen, J.; Jin, W. Q. A Graphene Oxide Membrane with Highly Selective Molecular Separation of Aqueous Organic Solution. *Angew. Chem., Int. Ed.* **2014**, *53*, 6929−6932.

(5) Sumboja, A.; Foo, C. Y.; Wang, X.; Lee, P. S. Large Areal Mass, Flexible and Free-Standing Reduced Graphene Oxide/Manganese Dioxide Paper for Asymmetric Supercapacitor Device. *Adv. Mater.* **2013**, *25*, 2809−2815.

(6) Huang, J. Q.; Zhuang, T. Z.; Zhang, Q.; Peng, H. J.; Chen, C. M.; Wei, F. Permselective Graphene Oxide Membrane for Highly Stable and Anti-Self-Discharge Lithium-Sulfur Batteries. *ACS Nano* **2015**, *9*, 3002−3011.

(7) Nair, R.; Wu, H.; Jayaram, P.; Grigorieva, I.; Geim, A. Unimpeded Permeation of Water through Helium-Leak-Tight Graphene-Based Membranes. *Science* **2012**, *335*, 442−444.

(8) Mi, B. Graphene Oxide Membranes for Ionic and Molecular Sieving. *Science* **2014**, *343*, 740−742.

(9) Rundquist, E. M.; Pink, C. J.; Livingston, A. G. Organic Solvent Nanofiltration: A Potential Alternative to Distillation for Solvent Recovery from Crystallisation Mother Liquors. *Green Chem.* **2012**, *14*, 2197−2205.

(10) Huang, L.; Chen, J.; Gao, T. T.; Zhang, M.; Li, Y. R.; Dai, L. M.; Qu, L. T.; Shi, G. Q. Reduced Graphene Oxide Membranes for

Ultrafast Organic Solvent Nanofiltration. *Adv. Mater.* **2016**, *28*, 8669−8674.
(11) Yang, Q.; Su, Y.; Chi, C.; Cherian, C. T.; Huang, K.; Kravets, V. G.; Wang, F. C.; Zhang, J. C.; Pratt, A.; Grigorenko, A. N.; Guinea, F.; Geim, A. K.; Nair, R. R. Ultrathin Graphene-Based Membrane with Precise Molecular Sieving and Ultrafast Solvent Permeation. *Nat. Mater.* **2017**, *16*, 1198−1202.
(12) Li, W. B.; Wu, W. F.; Li, Z. J. Controlling Interlayer Spacing of Graphene Oxide Membranes by External Pressure Regulation. *ACS Nano* **2018**, *12*, 9309−9317.
(13) Zheng, S.; Tu, Q.; Urban, J. J.; Li, S.; Mi, B. Swelling of Graphene Oxide Membranes in Aqueous Solution: Characterization of Interlayer Spacing and Insight into Water Transport Mechanisms. *ACS Nano* **2017**, *11*, 6440−6450.
(14) Joshi, R. K.; Carbone, P.; Wang, F. C.; Kravets, V. G.; Su, Y.; Grigorieva, I. V.; Wu, H. A.; Geim, A. K.; Nair, R. R. Precise and Ultrafast Molecular Sieving through Graphene Oxide Membranes. *Science* **2014**, *343*, 752−754.
(15) Szekely, G.; Jimenez-Solomon, M. F.; Marchetti, P.; Kim, J. F.; Livingston, A. G. Sustainability Assessment of Organic Solvent Nanofiltration: From Fabrication to Application. *Green Chem.* **2014**, *16*, 4440−4473.
(16) Talyzin, A. V.; Hausmaninger, T.; You, S.; Szabó, T. The Structure of Graphene Oxide Membranes in Liquid Water, Ethanol and Water-Ethanol Mixtures. *Nanoscale* **2014**, *6*, 272−281.
(17) Wei, N.; Lv, C.; Xu, Z. Wetting of Graphene Oxide: A molecular Dynamics Study. *Langmuir* **2014**, *30*, 3572−3578.
(18) Wang, Z. Y.; Tu, Q. S.; Zheng, S. X.; Urban, J. J.; Li, S. F.; Mi, B. X. Understanding the Aqueous Stability and Filtration Capability of MoS_2 Membranes. *Nano Lett.* **2017**, *17*, 7289−7298.
(19) Kim, J. E.; Han, T. H.; Lee, S. H.; Kim, J. Y.; Ahn, C. W.; Yun, J. M.; Kim, S. O. Graphene Oxide Liquid Crystals. *Angew. Chem., Int. Ed.* **2011**, *50*, 3043−3047.
(20) Li, D.; Muller, M. B.; Gilje, S.; Kaner, R. B.; Wallace, G. G. Processable Aqueous Dispersions of Graphene Nanosheets. *Nat. Nanotechnol.* **2008**, *3*, 101−105.
(21) Liu, R.; Arabale, G.; Kim, J.; Sun, K.; Lee, Y.; Ryu, C.; Lee, C. Graphene Oxide Membrane for Liquid Phase Organic Molecular Separation. *Carbon* **2014**, *77*, 933−938.
(22) Klechikov, A.; Yu, J.; Thomas, D.; Sharifi, T.; Talyzin, A. V. Structure of Graphene Oxide Membranes in Solvents and Solutions. *Nanoscale* **2015**, *7*, 15374−15384.
(23) Wei, N.; Peng, X. S.; Xu, Z. P. Understanding Water Permeation in Graphene Oxide Membranes. *ACS Appl. Mater. Interfaces* **2014**, *6*, 5877−5883.
(24) Tsukahara, T.; Hibara, A.; Ikeda, Y.; Kitamori, T. NMR Study of Water Molecules Confined in Extended Nanospaces. *Angew. Chem., Int. Ed.* **2007**, *46*, 1180−1183.
(25) Boukhvalov, D. W.; Katsnelson, M. I.; Son, Y. W. Origin of Anomalous Water Permeation through Graphene Oxide Membrane. *Nano Lett.* **2013**, *13*, 3930−3935.
(26) Huang, H. B.; Song, Z. G.; Wei, N.; Shi, L.; Mao, Y. Y.; Ying, Y. L.; Sun, L. W.; Xu, Z. P.; Peng, X. S. Ultrafast Viscous Water Flow through Nanostrand-Channelled Graphene Oxide Membranes. *Nat. Commun.* **2013**, *4*, 2979.
(27) Jiao, S. P.; Zhou, K.; Wu, M. M.; Li, C.; Cao, X. L.; Zhang, L.; Xu, Z. P. Confined Structures and Selective Mass Transport of Organic Liquids in Graphene Nanochannels. *ACS Appl. Mater. Interfaces* **2018**, *10*, 37014−37022.
(28) Hu, M.; Mi, B. Layer-by-Layer Assembly of Graphene Oxide Membranes *via* Electrostatic Interaction. *J. Membr. Sci.* **2014**, *469*, 80−87.
(29) Pines, E.; Fleming, G. R. Proton Transfer in Mixed Water-Organic Solvent Solutions: Correlation between Rate, Equilibrium Constant, and the Proton Free Energy of Transfer. *J. Phys. Chem.* **1991**, *95*, 10448−10457.
(30) Vanderhoeven, P. H. C.; Lyklema, J. Electrostatic Stabilization in Non-Aqueous Media. *Adv. Colloid Interface Sci.* **1992**, *42*, 205−277.
(31) Sarmini, K.; Kenndler, E. Ionization Constants of Weak Acids and Bases in Organic Solvents. *J. Biochem. Biophys. Methods* **1999**, *38*, 123−137.
(32) Valko, I. E.; Siren, H.; Riekkola, M. L. Characteristics of Electroosmotic Flow in Capillary Electrophoresis in Water and in Organic Solvents without Added Ionic Species. *J. Microcolumn Sep.* **1999**, *11*, 199−208.
(33) Vandezande, P.; Gevers, L. E. M.; Vankelecom, I. F. J. Solvent Resistant Nanofiltration: Separating on a Molecular Level. *Chem. Soc. Rev.* **2008**, *37*, 365−405.
(34) Machado, D. R.; Hasson, D.; Semiat, R. Effect of Solvent Properties on Permeate Flow through Nanofiltration Membranes - Part II. Transport Model. *J. Membr. Sci.* **2000**, *166*, 63−69.
(35) Dikin, D. A.; Stankovich, S.; Zimney, E. J.; Piner, R. D.; Dommett, G. H.; Evmenenko, G.; Nguyen, S. T.; Ruoff, R. S. Preparation and Characterization of Graphene Oxide Paper. *Nature* **2007**, *448*, 457.
(36) Bacon, G. E. The Interlayer Spacing of Graphite. *Acta Crystallogr.* **1951**, *4*, 558−561.
(37) Bondi, A. Van der Waals Volumes and Radii. *J. Phys. Chem.* **1964**, *68*, 441−451.
(38) Akbari, A.; Meragawi, S. E.; Martin, S. T.; Corry, B.; Shamsaei, E.; Easton, C. D.; Bhattacharyya, D.; Majumder, M. Solvent Transport Behavior of Shear Aligned Graphene Oxide Membranes and Implications in Organic Solvent Nanofiltration. *ACS Appl. Mater. Interfaces* **2018**, *10*, 2067−2074.
(39) Zheng, S.; Mi, B. Emerging Investigators Series: Silica-Crosslinked Graphene Oxide Membrane and Its Unique Capability in Removing Neutral Organic Molecules from Water. *Environ. Sci.: Water Res. Technol.* **2016**, *2*, 717−725.
(40) Marchetti, P.; Jimenez Solomon, M. F.; Szekely, G.; Livingston, A. G. Molecular Separation with Organic Solvent Nanofiltration: A Critical Review. *Chem. Rev.* **2014**, *114*, 10735−10806.
(41) Tarleton, E. S.; Robinson, J. P.; Smith, S. J.; Na, J. J. W. New Experimental Measurements of Solvent Induced Swelling in Nano-filtration Membranes. *J. Membr. Sci.* **2005**, *261*, 129−135.
(42) Murray, R. S.; Quirk, J. P. The Physical Swelling of Clays in Solvents. *Soil Sci. Soc. Am. J.* **1982**, *46*, 865−868.
(43) Brown, K. W.; Thomas, J. C. A Mechanism by Which Organic Liquids Increase the Hydraulic Conductivity of Compacted Clay Materials. *Soil Sci. Soc. Am. J.* **1987**, *51*, 1451−1459.
(44) Chen, S. Z.; Low, P. F.; Cushman, J. H.; Roth, C. B. Organic Compound Effects on Swelling and Flocculation of Upton Montmorillonite. *Soil Sci. Soc. Am. J.* **1987**, *51*, 1444−1450.
(45) Brindley, G. W. Intracrystalline Swelling of Montmorillonites in Water-Dimethylsulfoxide Systems. *Clays Clay Miner.* **1980**, *28*, 369−372.
(46) Siffert, B.; Jada, A.; Letsango, J. E. Location of the Shear Plane in the Electric Double Layer in an Organic Medium. *J. Colloid Interface Sci.* **1994**, *163*, 327−333.
(47) Parsons, R. The Electrical Double Layer in Non-aqueous Solvents. *Electrochim. Acta* **1976**, *21*, 681−686.
(48) Andecochea Saiz, C.; Darvishmanesh, S.; Buekenhoudt, A.; Van der Bruggen, B. Shortcut Applications of the Hansen Solubility Parameter for Organic Solvent Nanofiltration. *J. Membr. Sci.* **2018**, *546*, 120−127.
(49) Mertens, M.; Van Goethem, C.; Thijs, M.; Koeckelberghs, G.; Vankelecom, I. F. J. Crosslinked PVDF-Membranes for Solvent Resistant Nanofiltration. *J. Membr. Sci.* **2018**, *566*, 223−230.
(50) Postel, S.; Schneider, C.; Wessling, M. Solvent Dependent Solute Solubility Governs Retention in Silicone Based Organic Solvent Nanofiltration. *J. Membr. Sci.* **2016**, *497*, 47−54.
(51) Graber, E. R.; Mingelgrin, U. Clay Swelling and Regular Solution Theory. *Environ. Sci. Technol.* **1994**, *28*, 2360−2365.
(52) Hildebrand, J. H. A History of Solution Theory. *Annu. Rev. Phys. Chem.* **1981**, *32*, 1−23.
(53) Konios, D.; Stylianakis, M. M.; Stratakis, E.; Kymakis, E. Dispersion Behaviour of Graphene Oxide and Reduced Graphene Oxide. *J. Colloid Interface Sci.* **2014**, *430*, 108−112.

https://dx.doi.org/10.1021/acsnano.0c01550
ACS Nano 2020, 14, 6013−6023

(54) Boiadjiev, S. E.; Anstine, D. T.; Maverick, E.; Lightner, D. A. Hydrogen Bonding and π-Stacking in Dipyrrinone Acid Dimers of Xanthobilirubic Acid and Chiral Analogs. *Tetrahedron: Asymmetry* **1995**, *6*, 2253−2270.
(55) Mi, B.; Zheng, S.; Tu, Q. 2D Graphene Oxide Channel for Water Transport. *Faraday Discuss.* **2018**, *209*, 329−340.

https://dx.doi.org/10.1021/acsnano.0c01550
ACS Nano 2020, 14, 6013−6023